Spring 5-15-2020

# CFD Evaluation of Blood Flow in an Improved Blalock-Taussig Shunt Using Patient Specific Geometries

Zhenghao Lin
*Washington University in St. Louis*

WASHINGTON UNIVERSITY IN ST. LOUIS

James Mckelvey School of Engineering

Department of Mechanical Engineering and Materials Science

Thesis Examination Committee

Dr. Ramesh K. Agarwal, Chair

Dr. David Peters

Dr. Swami Karunamorthy

# CFD Evaluation of Blood Flow in an Improved Blalock-Taussig Shunt Using Patient Specific Geometries

by

Zhenghao Lin

A thesis presented to James Mckelvey School of Engineering

of Washington University in St. Louis in partial fulfillment of the

requirements for the degree of Master of Science

May 2020

Saint Louis, Missouri

# Table of Contents

# List of Figures

# List of Tables

# Nomenclature

| | |
|---|---|
| CHD | Cardiovascular Heart Disease |
| BT Shunt | Blalock – Taussig Shunt |
| mBTS | Modified Blalock – Taussig Shunt |
| CAD | Computer-Aided Design |
| CFD | Computational Fluid Dynamics |
| HHA | Hess-Hoganson-Agarwal |
| IA | Innominate Artery |
| PA | Pulmonary Artery |
| MPA | Main Pulmonary Artery |
| LCA | Left Carotid Artery |
| LSA | Left Subclavian Artery |
| WSS | Wall Shear Stress |
| RANS | Reynolds-Averaged Navier-Stokes Equations |

# Acknowledgements

I would like to express my sincere gratitude to those who helped me during my research in Computation Fluid Dynamics laboratory.

My deepest gratitude goes foremost to Professor Ramesh Agarwal for his inspiration, encouragement and guidance throughout my research. His knowledge, experience and patience have helped me to accomplish my research project and thesis in an excellent manner. Without him I would not have the opportunity to explore the academic world of Computation Fluid Dynamics (CFD).

Secondly, I would like to express my gratitude to several specialists at Boston Children's hospital, namely Dr. Vijay Govindarajan, Dr. Noah Schulz, and Dr. David Hoganson M.D who provided the patient specific model and helped in generating a suitable model for simulation, and in many helpful discussions.

Fianlly, I would like to acknowledge the help of Jeffery Krampf and Leilei Ji of CFD lab for helping with several aspects of the project.

Zhenghao Lin

Washington University in St. Louis
May 2020

Dedicated to my family

**Abstract**

**CFD Evaluation of Blood Flow in an Improved Blalock-Taussig Shunt Using Patient Specific Geometries**

By

Zhenghao Lin

Master of Science in Mechanical Engineering
Washington University in St. Louis

Research Advisor: Professor Ramesh K. Agarwal

Blalock-Taussig (BT) Shunt is a palliative surgical procedure used during a Norwood surgery on a new born baby suffering from cyanotic heart defects. The BT Shunt can increase blood flow in patients' pulmonary artery which can ease the "Blue Baby Syndrome." Currently used BT Shunts do not produce a balanced flow distribution to the pulmonary arteries (PAs) which can cause high wall shear stress (WSS) and blood flow separation resulting in blood clots. A modified BT Shunt is designed to partially solve this problem. It is shown by numerical simulations that modified BT Shunt has the ability to better control the flow distribution between Innominate Artery (IA) and PA with lower and gradually varying WSS and with improved flow balance to the pulmonary artery at the T-junction of the shunt. The main goal of this thesis is to computationally evaluate the flow in the modified BT shunt model between innominate and pulmonary artery using a patient specific aorta model. The simulations are performed using the commercial CFD software ANSYS Fluent. The improved modified BT shunt is connected between IA and PA. A change in the length of the shunt can be made to fit it under different conditions of actual patients. In numerical simulations, a full geometry of patient's aorta is considered. Results for different length of the shunt are compared to determine the length that generates the lowest WSS and improved flow distribution to the PAs. It was found that the length of nearly 26mm creates

lower WSS as well as flow rate difference between the two sides of PA at the T-junction attachment of the shunt. A sophisticated computational model was created using Solidworks and Blender software to create the realistic geometry which included the IA, PA and modified BT shunt. The numerical simulations provide details of the flow field including velocity and pressure field, and WSS. Several parameters in shunt design weigh heavily in reducing the thrombosis. This study demonstrates how CFD can be effectively utilized in the design of a medical device such as BT shunt to improve the clinical outcomes in patients.

# Chapter 1 Introduction

## 1.1 Blue Baby Syndrome and Cyanotic Heart Disease

The Blue Baby Syndrome refers to a newborn infant (normally less than four weeks of age) with a purple or blue skin color. This syndrome is generally caused by the low transport of oxygen due to decreased hemoglobin in the blood. There are mainly two causes of the syndrome: Cyanotic heart disease (CHD) and Methemoglobinemia. In this thesis, we focus on the cyanotic heart disease which results in the Blue Baby Syndrome.

Cyanotic heart disease is an important cause of infant mortality. The cyanosis can occur when the infant has pulmonary atresia; pulmonary stenosis; aortic transposition; tricuspid atresia; tetralogy of Fallot; permanent arterial stem; ectopic drainage of pulmonary veins and sabnormal pulmonary venous return. The cyanosis indicates that hypoxia in the body may cause damage to important organs such as the brain, heart, kidney, and lungs of the newborns, thereby affecting their and overall physical development.

## 1.2 Blalock Taussig Shunt Overview

The Blalock-Taussig (BT) shunt provides a surgical solution for infants who suffer from "Blue Baby Syndrome" which is due to insufficient blood supply from heart to lungs in a newborn baby. The syndrome occurs when there exists an abnormal tunnel between heart and lungs and the irregular shape of the vessel can cause a significant decrease in transporting blood from heart to lungs. A more serious effect occurs if a newborn baby suffers from hypoxia. Unfortunately, a major surgery requiring the rebuilding of the blood vessel is nearly impossible for a very young child. Therefore, a palliative procedure is employed until definitive repairs can be made by a surgical procedure.

Surgery using a BT shunt was first performed by Dr. Helen Brooke Taussig, Dr. Alfred Blalock and Dr. Vivien Thomas. The aim of the surgery was to connect either the subclavian or the carotid artery to one side of the pulmonary artery as shown in Fig. 1.1. A BT shunt is a cylindrical tube made from a bio- material called Gore-Tex. The shunt inflates and shrinks due to blood pressure similar to a real blood vessel. The BT shunt typically has a diameter from 3 to 4 millimeters depending on the size and age of the child.

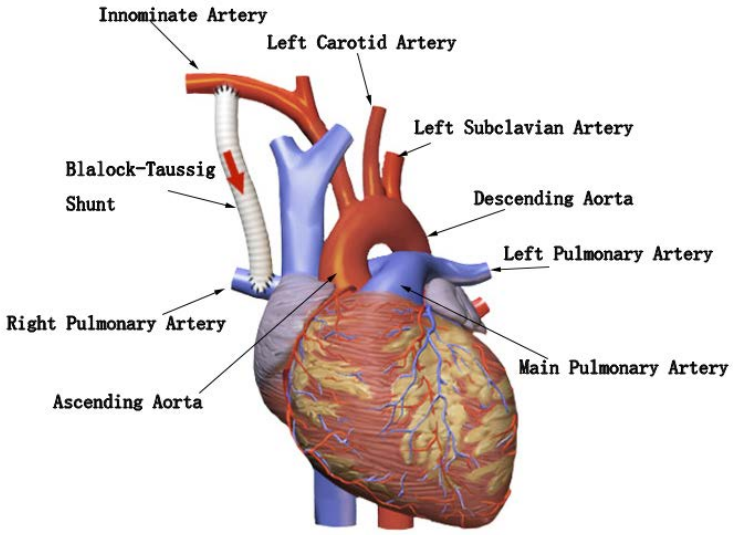


Figure 1.2 Blalock-Taussig Shunt: It is attached from Right Innominate Artery to Right Pulmonary Artery

## 1.3 Motivation

This study conducts the numerical simulations of blood flow in a patient-specific geometry using a recently modified BT Shunt (mBTS), also called the Hess-Hoganson-Agarwal (HHA) shunt[2] to evaluate its performance in achieving the desired blood flow in two lungs. In Reference [2], it was shown that the mBTS (HHA Shunt) had excellent properties of gradually varying wall-shear-stress (WSS) as well as nearly equal distribution of blood flow in right and left pulmonary arteries. This shunt has been used in this study with minor changes in its length to fit the innominate and pulmonary arteries.

## 1.4 Brief Review of Literature

Study of the hemodynamics of BT Shunts developed over past several decades has been a significant topic of research. In spite of major developments, there is still a need for improvement to reduce the morbidity rate. In a 2011 study, 1273 patients' data were analyzed for post operation performance of BT Shunts. It was found that there was an overall 13.1% chance of morbidity with 33% of deaths occurring within 24 hours and 75% within the first month. The study concluded that the mortality rate after the implementation of BT Shunts remained high, especially for infants under the weight of 3 kg or with a diagnosis of pulmonary atresia with intact ventricular septum (PA/IVS) [3].

Modern BT Shunt use Gore-Tex material for creating an artificial vessel, while older generation of prosthetic grafts caused in some cases non-physiologic flow resulting in stenosis or thrombosis in shunts. The Gore-Tex artificial blood vessels are now used for parts that need to be replaced or bridged due to stenosis, hemangioma, trauma, etc. It is also used for other types of vascular surgery such as Arteriovenous Fistula (AVF). In a 1982 study, eight patients used BT Shunts with Gore-Tex. It turned out that the all patients were free from morbidity [4]. Recently, umbilical vein segments in place of Gore-Tex material are being considered for graft material to provide a closer resemblance to blood vessels in order to lower the chance for foreign material rejection by the body.

## 1.5 Scope of the Thesis

The main goal of the thesis is to evaluate the performance of a newly modified BT Shunt (mBTS) – the HHA Shunt by installing in a patient specific geometry and performing the numerical simulations. In numerical simulations, several assumptions are made: (1) the walls of the model geometry are rigid and smooth, (2) the blood is a Newtonian fluid [5-7] with a density of 1060 kg/m3 and viscosity of 0.0035 kg/ms, and (3) the flow boundary conditions are set by using the average values from accrued patient data. The flow conditions used are also from patient data which are an average of several patients' data. The aorta model used in

the study was provided by the Boston Children's Hospital group as a 3D scan and the assembly of the shunt with aorta model was accomplished by using the Blender software. The model was then converted into a rigid body model using AutoDesk Fusion 360 and was meshed using ANSYS Workbench. The simulation was conducted using the ANSYS Fluent and the numerical data was processed using ANSYS CFD Post. Reynolds-Averaged Navier-Stokes (RANS) equations with k-kl-$\omega$ transitional flow model were solved using the finite-volume method in Fluent. PRESTO! numerical algorithm was used for pressure-velocity coupling. In Fluent, convection terms in RANS were discretized using a third-order upwind scheme while diffusion terns were central–differenced by a second-order scheme. All simulation data was recorded using Microsoft Excel and then post-processed using CFD Post.

# Chapter 2 Computational Methodology

## 2.1 Overview

The objective of this thesis is to evaluate the performance of a recently modified BT shunt (HHA Shunt) [2] installed in a patient specific model by numerical simulation. A good BT Shunt should have (1) a lower overall maximum WSS, (2) a smooth transition between high and low WSS, (3) a minimal amount of flow separation, (4) an equivalent effective resistance of modern shunts, and (5 )an even flow distribution to the left and right lung. Against these performance criteria, the performance of HHA Shunt is studied in a patient specific geometry by numerical simulations.

The model was built in Solidworks using CAD files. The four boundary conditions were provided by surgery data.

## 2.2 Computational Fluid Dynamics

Computational fluid dynamics (CFD) is a field of fluid mechanics that employs numerical methods and data structures to solve the governing equations of fluid flow that best describe the fluid physics for a given application. CFD is a powerful tool for analysis and design of fluid systems but requires enormous computing power for complex 3D applications.

Most CFD simulations generally go through three phases: pre-processing, flow field simulation, and post-processing of numerical data. During pre-processing the geometry of the system is defined by importing a predefined CAD file which needs to be cleaned up to define the smooth geometry and the surrounding fluid domain. This fluid domain is then divided into discrete cells called the mesh. The mesh can be unstructured or structured consisting of pyramidal or polyhedral cells respectively. The mesh is typically finer in areas of high gradients of flow variables, e.g. near walls, and swirling flow regions.

In the simulation phase, the appropriate governing equations of fluid flow are discretized on the generated mesh by utilizing a proper numerical algorithm. The computer then solves the discretized equations for the unknown flow variables for each cell of the mesh. A suitable algorithm is selected for each equation to ensure accuracy and stability. In the final phase, the numerical data is post processed in the form of flow quantities that can be used to evaluate the performance of a device/product as well as to display the flow variables in the domain in the form of contours.

## 2.2.1 Governing Equations

In order to describe fluid flow, three partial differential equations are used: the conservation of mass (continuity equation), the conservation of momentum, and the conservation of energy. When the flow is turbulent additional transport equations for turbulence model are also solved. The conservation equations can be written as [8]:

Continuity equation:

$$\frac{\partial \rho}{\partial \mathrm{t}} + \frac{\partial}{\partial x_i}(\rho u_i) = 0 \tag{2-1}$$

Momentum equation:

$$\frac{\partial}{\partial t}(\rho u_i) + \frac{\partial}{\partial x_i}(\rho u_i u_j) = -\frac{\partial p}{\partial x_i} + \frac{\partial \tau_{ij}}{\partial x_i} \tag{2-2}$$

Energy equation:

$$\frac{\partial}{\partial t}\left[\rho\left(h + \tfrac{1}{2}{u_i}^2\right)\right] + \frac{\partial}{\partial x_i}\left[\rho u_j\left(h + \tfrac{1}{2}{u_i}^2\right)\right] = \frac{\partial p}{\partial \mathrm{t}} + \frac{\partial}{\partial x_j}\left(u_i \tau_{ij} + \lambda \frac{\partial T}{\partial x_j}\right) \tag{2-3}$$

where $\tau_{ij}$ the stress tensor and $h$ the enthalpy given as:

$$\tau_{ij} = \mu\left(\frac{\partial u_i}{\partial x_j} + \frac{\partial u_j}{\partial x_i}\right) - \frac{2}{3}\mu \frac{\partial u_i}{\partial x_i}\,\delta_{ij} \tag{2-4}$$

$$h = C_p T \tag{2-5}$$

The above governing equations are solved as a coupled system of five non-linear partial differential equations with six unknown flow-field variables $u$, $v$, $w$, $p$, $\rho$, and $T$. Another equation relating temperature, pressure, and density is provided by the equation of state of a given fluid.

## 2.2.2 Turbulence Models

Turbulent flow is defined as any fluid motion characterized by chaotic changes in pressure or flow velocity [9]. While most of the flows in the real world can be considered as turbulent flows, many consist of a combination of laminar, transitional, and turbulent flows. The onset of turbulence can be predicted by a dimensionless parameter, the Reynolds number. The small fluctuations in velocity, pressure, and temperature fields in turbulent flow result in changes in transport quantities such as the momentum and energy of the system.

Since small fluctuations in turbulent flows are difficult to model due to their chaotic nature, simplifications are generally made to the governing equations of fluid dynamics in order to solve them on currently available computer for 3D industrial applications. One of the most widely used approximations is obtained by time-averaging the equations which result in the so called Reynolds Averaged Navier Stokes (RANS) equations. Turbulence models are used to model the unknown "Reynolds Stresses" in the RANS equations. Unfortunately, no single turbulence model can accurately solve all turbulent flow problems. Therefore, a wide variety of turbulence models have been proposed in the literature over a century. In this thesis, we consider the k-kl-ω model since it is applicable for computing the transitional flows [10].

k-kl-ω model is a three-equation eddy-viscosity type turbulence model where the three transport equations for turbulent kinetic energy ($k_T$), laminar kinetic energy ($k_L$) and inverse turbulence time scale ($\omega$) are given as:

$$\frac{Dk_T}{D\mathrm{t}} = P_{k_T} + R + R_{NAT} - \omega k_T - D_T + \frac{\partial}{\partial x_j}\left[\left(v + \frac{\propto_T}{\propto_k}\right)\frac{\partial k_T}{\partial x_j}\right] \tag{2-6}$$

$$\frac{Dk_L}{D\mathrm{t}} = P_{k_L} + R + R_{NAT} - D_L + \frac{\partial}{\partial x_j}\left[v\frac{\partial k_L}{\partial x_j}\right] \tag{2-7}$$

$$\frac{D\omega}{D\mathrm{t}} = C_{\omega 1}\frac{\omega}{k_T}P_{k_T} + \left(\frac{C_{\omega R}}{f_W} - 1\right)\frac{\omega}{k_T}(R + R_{NAT}) - C_{\omega 2}\omega^2 + C_{\omega 3}f_\omega \alpha_T f_W^2 \frac{\sqrt{k_T}}{d^3} + \frac{\partial}{\partial x_j}\left[\left(v + \frac{\propto_T}{\propto_k}\right)\frac{\partial \omega}{\partial x_j}\right] \tag{2-8}$$

The turbulent sheer stresses and thermal stresses are defined by using the Boussinesq approximation via the eddy viscosity and turbulent thermal diffusivity as:

$$\overline{-u_i u_j} = v_{TOT}\left(\frac{\partial U_i}{\partial x_j} + \frac{\partial U_j}{\partial x_i}\right) - \frac{2}{3}k_{TOT}\delta_{ij} \tag{2-9}$$

$$\overline{-u_i \theta} = \alpha_{\theta,TOT}\frac{\partial \theta}{\partial x_i} \tag{2-10}$$

The effective length is characterized as:

$$\lambda_{eff} = MIN(C_\lambda d,\ \lambda_T) \tag{2-11}$$

where $\lambda_T$ is the turbulent length scale defined by:

$$\lambda_T = \frac{\sqrt{k}}{\omega} \tag{2-12}$$

with the small-scale kinetic energy defined by:

$$k_{T,s} = f_{ss} f_W k_T \tag{2-13}$$

$$f_W = \frac{\lambda_{eff}}{\lambda_T} \tag{2-14}$$

$$f_{ss} = exp\left[-\left(\frac{C_{ss} v \Omega}{k_T}\right)^2\right] \tag{2-15}$$

The large-scale energy kinetic is given by:

$$k_{T,l} = k_T - k_{T,s} \tag{2-16}$$

The turbulence production term generated by turbulent fluctuations is defined as:

$$P_{k_T} = v_{T,s} S^2 \tag{2-17}$$

where $v_{T,s}$ is the small-scale turbulent viscosity given as:

$$v_{T,s} = f_v f_{INT} C_\mu \sqrt{k_{T,s}} \lambda_{eff} \tag{2-18}$$

and

$$C_\mu = \frac{1}{A_o + A_s(S/\omega)} \tag{2-19}$$

$$f_v = 1 - exp\left(-\frac{\sqrt{R_{e_{T,s}}}}{A_v}\right) \tag{2-20}$$

A damping function defining the turbulence production due to intermittency is given by:

$$f_{INT} = MIN\left(\frac{k_L}{C_{INT} k_{TOT}}, 1\right) \tag{2-21}$$

$$R_{e_{T,s}} = \frac{f_W^2 k_T}{v_\omega} \tag{2-22}$$

where $P_{k_L}$ is the production of laminar kinetic energy by large scale turbulent fluctuations given by:

$$P_{k_L} = v_{T,l} S^2 \tag{2-23}$$

The large-scale turbulent viscosity $\boldsymbol{v_{T,l}}$ is modeled as:

$$v_{T,l} = MIN\left\{v^*_{T,l}, \frac{0.5(k_L + k_{T,L})}{s}\right\} \tag{2-24}$$

where

$$v^*_{T,l} = f_{\tau,1} C_{11} \left(\frac{\Omega \lambda^2_{eff}}{v}\right) \sqrt{f_{T,1}}\lambda_{eff} + \beta_{TS} C_{12} \phi_{NAT} d^2_{\Omega} \tag{2-25}$$

A full in-depth information on this turbulence model including the model constants is given in ANSYS Fluent 12.0 Theory Guide[8].

## 2.2.3 Discretization Methods

Now that the governing equations are defined in section 2.2.1 and 2.2.2, these equations need to be solved for a given geometry. However, the governing equations are highly non-linear and cannot be solved analytically except for a few cases of laminar flow in simple geometries. Therefore they are discretized on a given simulation model described in Chapter 3 and are solved numerically by using a CFD solver. Here we employ ANSYS Fluent.

The methods by which the PDEs are discretized are based on the mathematical character of the governing equations whether they are elliptic, parabolic, or hyperbolic. A suitable iterative numerical method such as the finite element method (FEM), finite difference method (FDM), or finite volume method (FVM) can be chosen to discretize the PDEs to obtain a set of algebraic equations. In this dissertation, FVM is employed.

FVM discretizes and solves the governing equations in integral form for each cell in the computational domain. The volume integral for each cell is converted into surface integral using of the divergence theorem as shown below in Eq. (2-26):

$$\iiint_V (\nabla \cdot \mathrm{F})\, \mathrm{d}V = \oiint_S \mathrm{F} \cdot \mathrm{dS} \tag{2-26}$$

The surface integrals in Eq. (2.26) are evaluated as flux integrals on the faces of the cells. Thus, in FVM, the Navier-Stokes equations, conservation of mass, conservation of energy, and turbulence model equations are all discretized and solved for each finite volume in the form shown below in Eq. (2-27).

$$\frac{\partial}{\partial t}\iiint Q dV + \iint F dA = 0 \tag{2-27}$$

where $Q$ is the vector of the conserved variables, $F$ is the flux vector, $dV$ is the volume of the cell, and $dA$ is the surface area of the cell [11].

## 2.2.4 Solution of the Discretized Equations

For solution of the discretized equations obtained by FVM, there are several solution methods available in a CFD solver such as Fluent. These methods include a choice of numerical scheme (non-coupled or coupled) and the order of spatial discretization of derivatives in the governing equations for accuracy and stability.

Algorithms can be uncoupled, where momentum equations and pressure corrections are solved separately, or coupled where both momentum equations and pressure corrections are solved simultaneously. The later requires more memory and CPU but provides higher accuracy. The coupled algorithm is chosen in this thesis, which obtains a robust and efficient solution for steady-state flows with superior performance compared to the uncoupled solution schemes [8].

In FVM, gradients and derivatives within a cell and cell faces are obtained using a number of approaches. Many different gradient solution methods are available including the Green-Gauss cell-based, Green-Gauss node-based, and Least Squares cell-based methods. In this study, the Green-Gauss node-based scheme, or GGNB, is used due to its increased accuracy compared to standard cell-based methods. The node-based approach was first proposed by Holmes and Connell who constructed the nodal values to be the weighted averages of the surrounding face values [12]. This scheme has high accuracy for unstructured meshes,

namely the triangular and tetrahedral meshes which are used in this thesis as described in Chapter 3. GGNB uses the following equation for computing the gradients:

$$\varphi_f = \frac{1}{N_f} \sum_n^{N_f} \varphi_n \tag{2-28}$$

where $\varphi_f$ is the gradient of scalar calculated at the face, $N_f$ is the number of nodes on the face, and $\varphi_n$ is the value calculated at each node. Figure 2.1 illustrates this scheme.

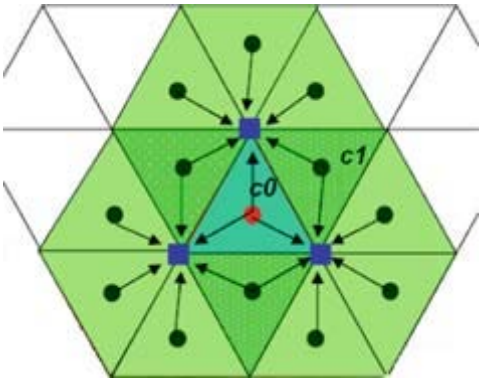


Figure 2.3 Green-Gauss Node-Based Gradient Based Solution Scheme [14]

When using a pressure-based solver, several different pressure interpolation schemes are available in Fluent such as standard, body-force-weighted, PRESTO!, and second-order scheme. These pressure interpolations are used to decide how the pressure gradient term is discretized. In this thesis, the PRESTO! scheme is chosen due to its accuracy for computing flows through curved domains and rotating flows. This scheme uses the discrete continuity balance for a "staggered" control volume about the face to compute the pressure on the face. This procedure is similar in spirit to the staggered-grid schemes used with structured meshes [8] [13]. PRESTO! avoids interpolation errors and pressure gradient assumptions near the boundaries of the geometry to provide higher accuracy in these areas. Figure 2.2 shows the PRESTO! scheme applied to staggered grid.

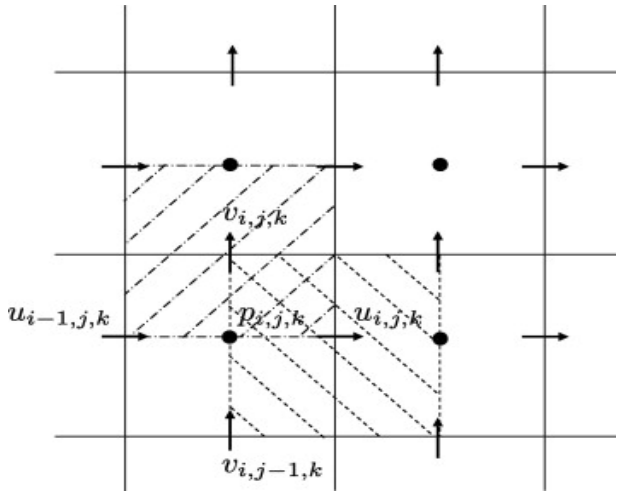


Figure 2.4 PRESTO! Pressure Interpolation Scheme [15]

### 2.2.5 Description of CFD Solver ANSYS Fluent

In this study the time-averaged Navier-Stokes equations, known as the Reynolds-averaged Navier-Stokes (RANS) equations are solved using Fluent, a commercial CFD program developed by ANSYS Inc. The Fluent software contains the flow modeling capabilities for turbulent flows and flows with heat transfer and chemical reactions for industrial and academic applications. The solver is FVM based software used on a collocated grid [8] with many different numerical schemes available which can be customizable based on a given application. It has several zero-, one- and two-equation turbulence models [11]. Fluent can compute both compressible and incompressible flows as well as both steady and unsteady flows. It has the option of several constitutive relations for modeling non-Newtonian flows. In Fluent, governing equations are solved on a structured or unstructured grid in a computational domain.

ICEM CFD is a software package that specializes in geometry modeling and mesh generation and is available in the ANSYS Workbench Suite. It is designed specifically for aerospace, automotive, and other engineering applications that require modeling and simulation of fluid flow using the tools of computational fluid dynamics. It can create geometries and excellent meshes automatically based on mesh controls. The meshing control

allows the generation of structured, unstructured, or hybrid grids with desired mesh size, refinement, inflation, face, and pinch functions. Any type of mesh, simple to complex, can be quickly generated using ICEM which is then imported to Fluent for calculation of the flow field.

# Chapter 3 Simulation Models-Geometry and Mesh Generation

## 3.1 Modified BT Shunt (mBTS) Model

As mentioned before, the goal of this thesis is to simulate the flow in mBTS (HHA shunt) to test its hemodynamic performance. Figure 3.1 and Figure 3.2 show the geometry of the original mBTS (HHA Shunt) and the extruded mBTS which has been used in this study. The original length of the shunt [1] is extruded from 18.54 mm to 24.50mm.

The original model was developed by Hess, Hoganson and Agarwal [HHA] [1]. It turns out that the length of the original HHA Shunt was 18.54 mm which is smaller to attach in a patient specific geometry which requires a shunt of length 24.5 mm. In order to fit the patient specific geometry between Innominate Artery (IA) and Pulmonary Artery (PA), an extruded shunt shown in Figure 3.2 was designed.

Figure 3.11 Original mBTS (HHA Shunt) with 18.54mm length [1]

Figure 3.12 Extruded HHA Shunt with 24.5mm length

# 3.2 Construction of Shunt Model from Patient Specific Geometry

## 3.2.1 Patient Specific Geometry

The patient specific geometry, shown in Fig. 3.3, was first imported as a STL file which means that the model was generated by vertices and edges. This geometry was provided by collaborators at Boston Children's hospital. It was substantially modified and simplified without affecting the evaluation of the performance of the mBTS.

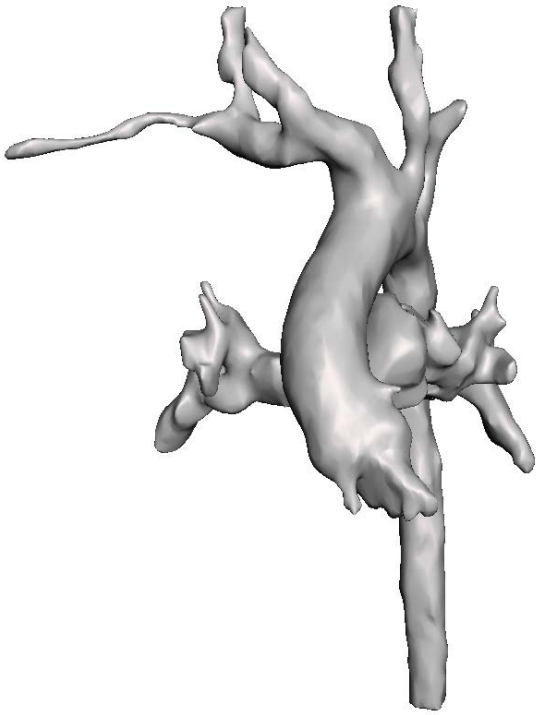

Figure 3.13 CT Scan of a Patient's Aorta Geometry

### 3.2.2 The Connection of Shunt in Geometry of Figure 3.3

The connection of the shunt in a real patient's aorta model with Innominate Artery (IA) and Pulmonary Artery (PA) is accomplished using the Blender software. A horizontal rotation is made to fit the shunt with IA and PA arteries as well as to create a better perspective for surgical purpose. Figure 3.4 shows how the IA and PA are connected by the shunt in the aorta model.

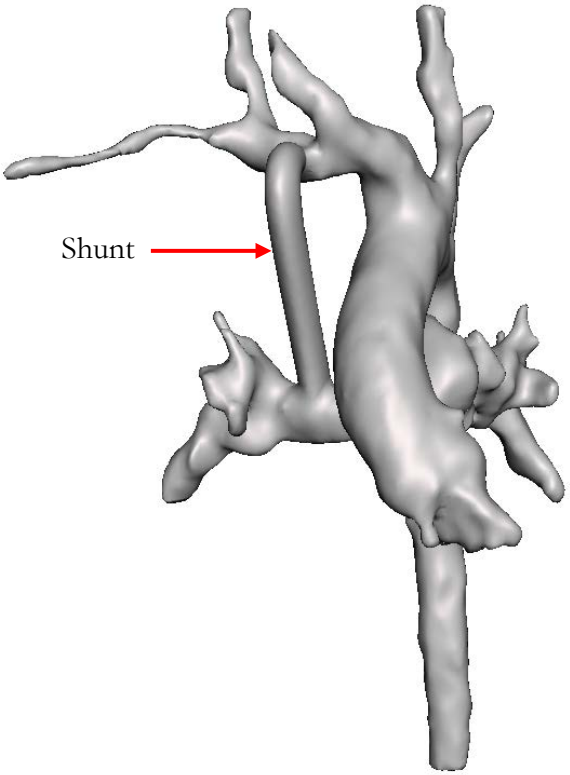


Figure 3.14 The Connection of the Shunt with PA and IA

### 3.2.3 Creation of a Simpler Model from Figure 3.4

As a first step in the flow simulations, a simpler model is created to reduce the complexity of the geometry shown in Fig. 3.4 and to study the hemodynamic performance of the shunt in a relatively simple model. Figures 3.5-3.10 show several steps employed in simplifying the geometry in Fig. 3.4 using the Blender Software. As shown in Fig. 3.9, only parts of the IA and PA are left in the original aorta model of Fig. 3.4, which are connected by the mBTS; this geometry is used in the numerical simulations reported in this thesis.

Figure 3.15 Trimming of the Patient Specific Aorta Model (Step 1 and 2): The Right IA was trimmed (Left) and the upper branch of IA was trimmed (Right)

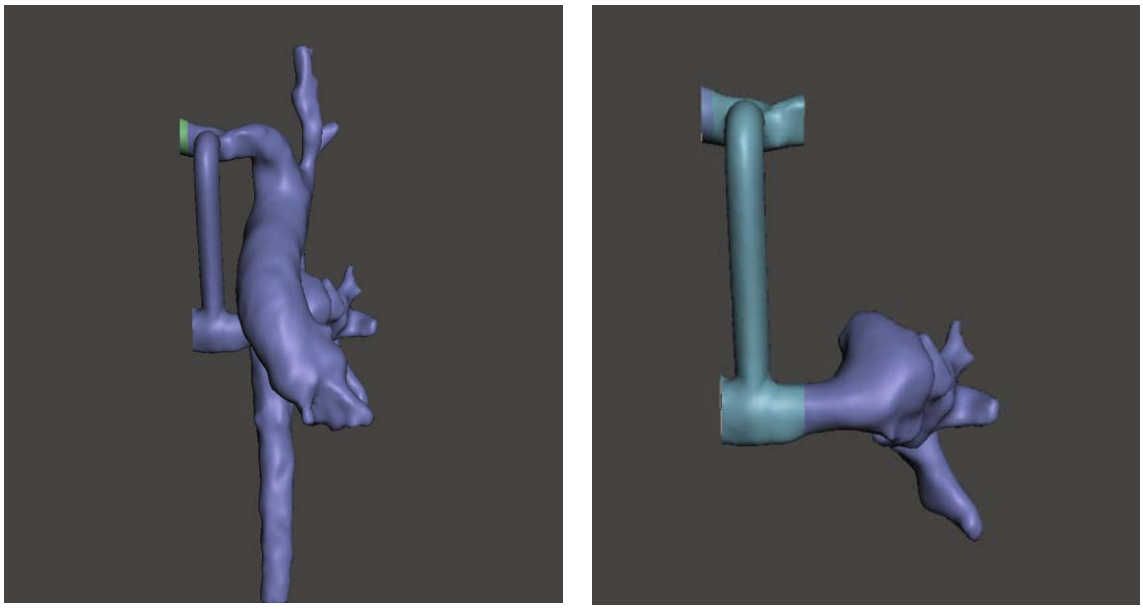

Figure 3.16 Trimming of the Patient Specific Aorta Model (Step 3 and 4): The Right PA was trimmed (Left) and the Aorta was trimmed (Right)

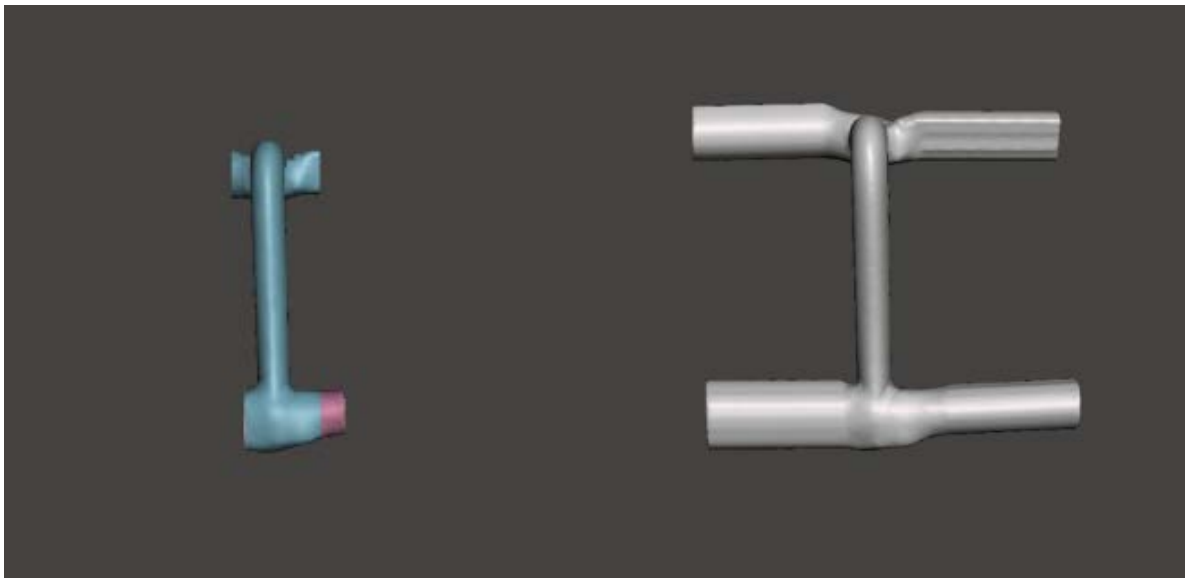

Figure 3.17 Trimming of the Patient Specific Shunt Model (Step 5 and 6): The Left PA was trimmed (Left) and the model was extruded from the model created in Step 5 (Right)

## 3.3 Construction of 3D Aorta Model including BT Shunt

The final 3D geometry of patient specific aorta model, shown in Fig. 3.8, was built to study the detailed flow field and other important parameters such as WSS and flow rates in Left Pulmonary Artery (LPA) and Right Pulmonary Artery (RPA) with the shunt installed connecting PA and IA. The outlet branches of the model were trimmed and were extruded for simulation.

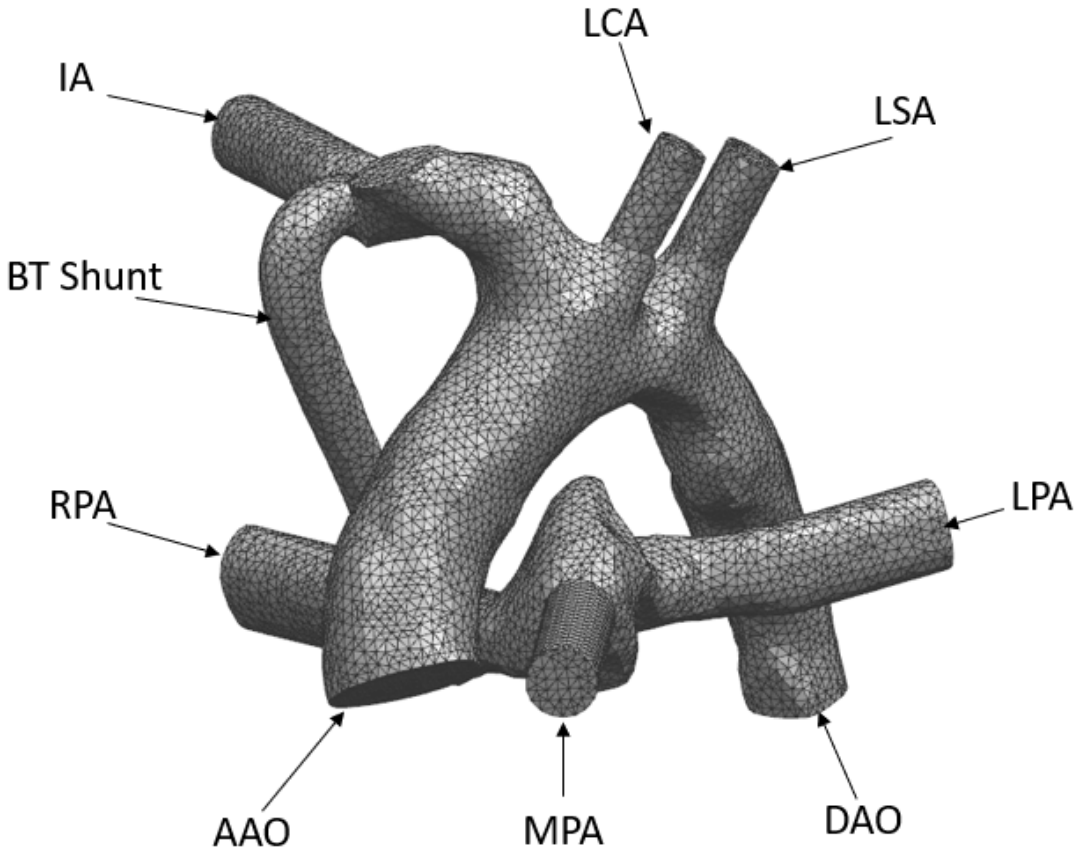


Figure 3.18 The Final 3D Aorta Model with BT Shunt/ It includes Innominate Artery (IA), BT-Shunt, Right Pulmonary Artery (RPA), Ascending Aorta (AAO), Main Pulmonary Artery (MPA), Descending Aorta (DAO), Left Pulmonary Artery (LPA), Left Subclavian Artery (LSA) and Left Carotid Artery (LCA)

# 3.4 Mesh Generation

## 3.4.1 Meshing of Extruded Model of BT Shunt in Fig. 3.7

The maximum dimension of the face during the meshing process was set at 1.3E-04m. Inflation layers were included to capture the flow near the boundaries accurately. The first

layer thickness from the boundary controls the first inflation layer, the number of layers, and the growth rate between each layer. The first layer height was set at 1.5E-6 meters, the maximum layers were set to 20, and the growth rate was set as default 1.2. Figure 3.9 shows the mesh inside the simple model. The model consisted of 1.8 million nodes and 5.5 million elements.

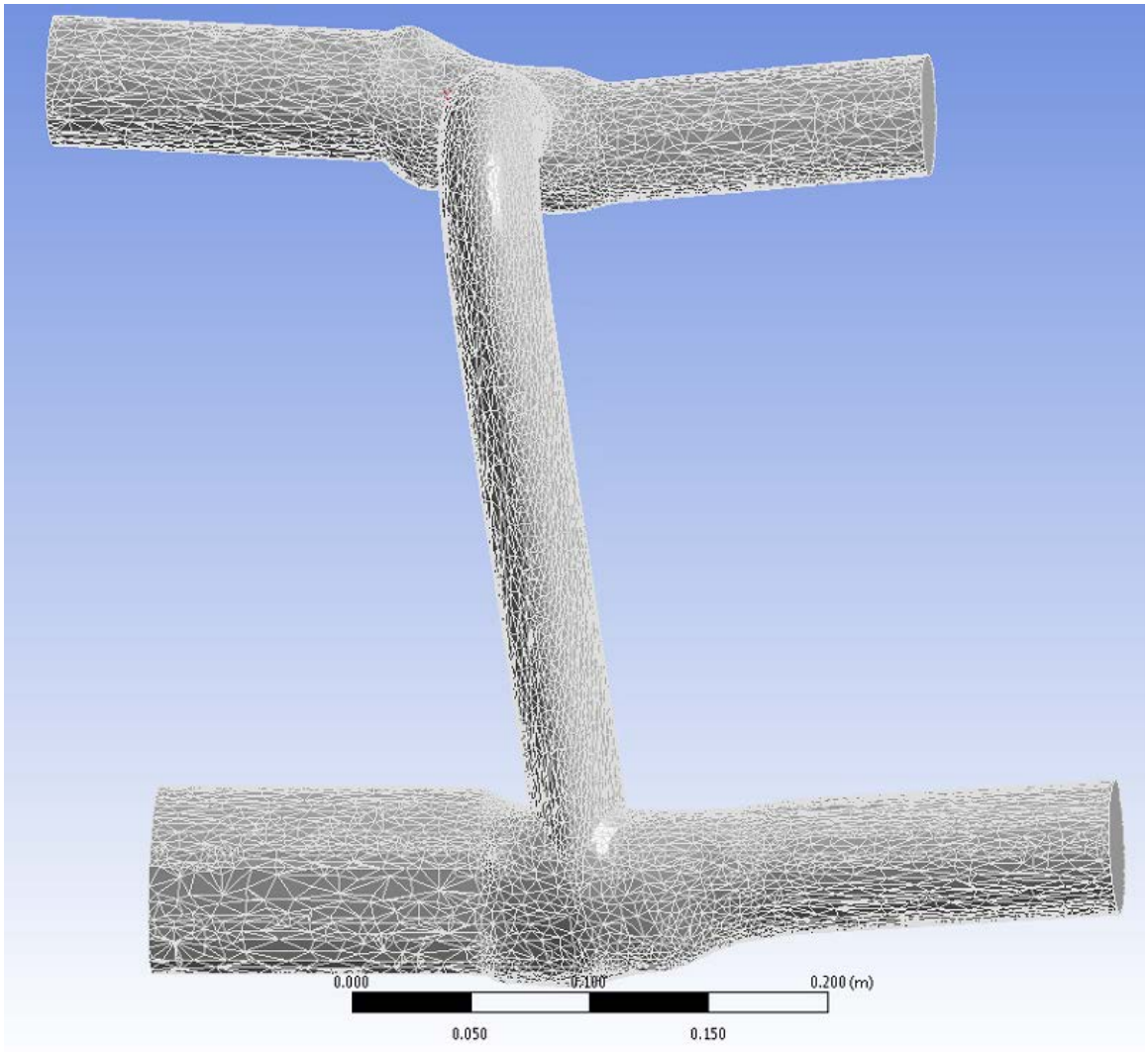


Figure 3.19 Mesh Inside the Simple Extruded Model of BT Shunt in Fig. 3.7

## 3.4.2 Meshing of 3D Aorta Model with BT Shunt

Three sets of grids were used with number of elements varying from 220 thousand (coarse) to 2.2 million (medium) to 5 million (fine) to conduct the mesh independent study of the

computed solution. The element size was 9E-04 (coarse mesh) to 3E-04 (fine mesh). The density of the mesh in the T-junction area of shunt joining LPA and RPA was increased to better capture the WSS distribution in the simulation. The inflation layer was set with a thickness of first layer equal to 5E-04 with 20 layers and 1.1 growth rate. Figure 3.10 shows the mesh of the model and details of the mesh at the face of Innominate Artery.

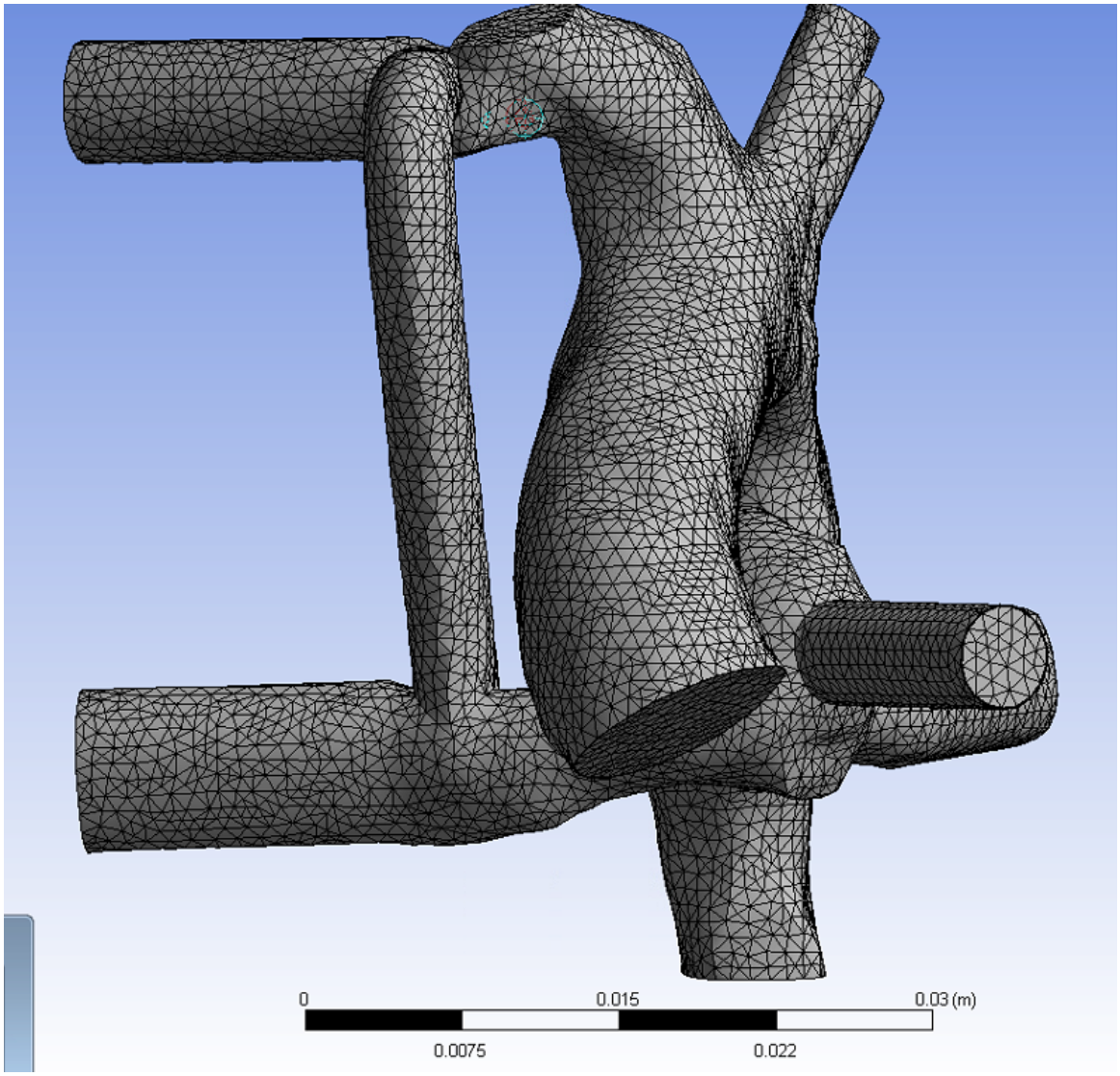

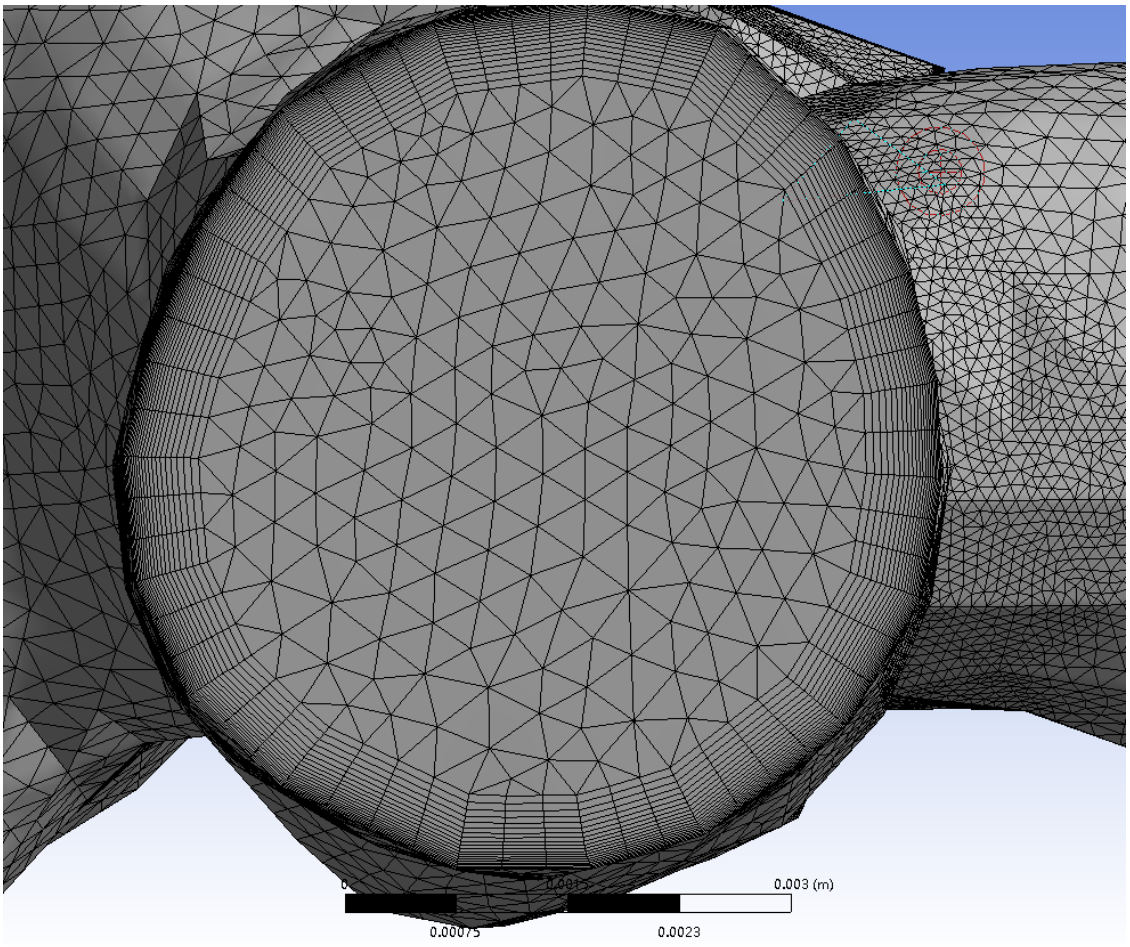


Figure 3.20 Mesh inside 3-D Aorta Model and zoomed- in view of Innominate Artery

# Chapter 4 Results and Discussion

## 4.1 Mesh Independence Study

There are multiple sources of error that can contribute to inaccuracy in the numerical solution: (a) Physical model (b) Turbulence model, (c) Mesh, and (d) Numerical algorithm. Once physical model, turbulence model and numerical algorithms have been decided by the user, it is very important that the solutions are grid independent since the density of the mesh can significantly affect the results of the simulation. The final validation of the computed solution is generally done against the experimental data. Since no experimental data is available in the present study, we performed the computations on a sequence of grids from coarse to fine to determine a suitable grid which gives accurate solutions (grid independent) and is also computationally efficient.

For grid independence study, the final 3-D patient specific aorta model was created as shown in Fig. 3.8 to run simulations on a sequence of grids and to determine the best grid from the point of view of both accuracy and efficiency. The mesh refinement focused primarily at the two BT shunt junctions in the model with IA and PA to obtain the WSS more accurately, whereas the mesh in the aorta and other parts of the arteries remained relatively unchanged from coarse to fine mesh in the mesh independent study. The velocity and pressure distribution at three most important parts of the model are shown in Fig. 4.1. One can see that the velocity magnitude at the centerline of the shunt is converging (i.e. the data of the coarsest mesh is approaching to the second refined mesh), and that difference is becoming smaller with the second mesh being further refined.

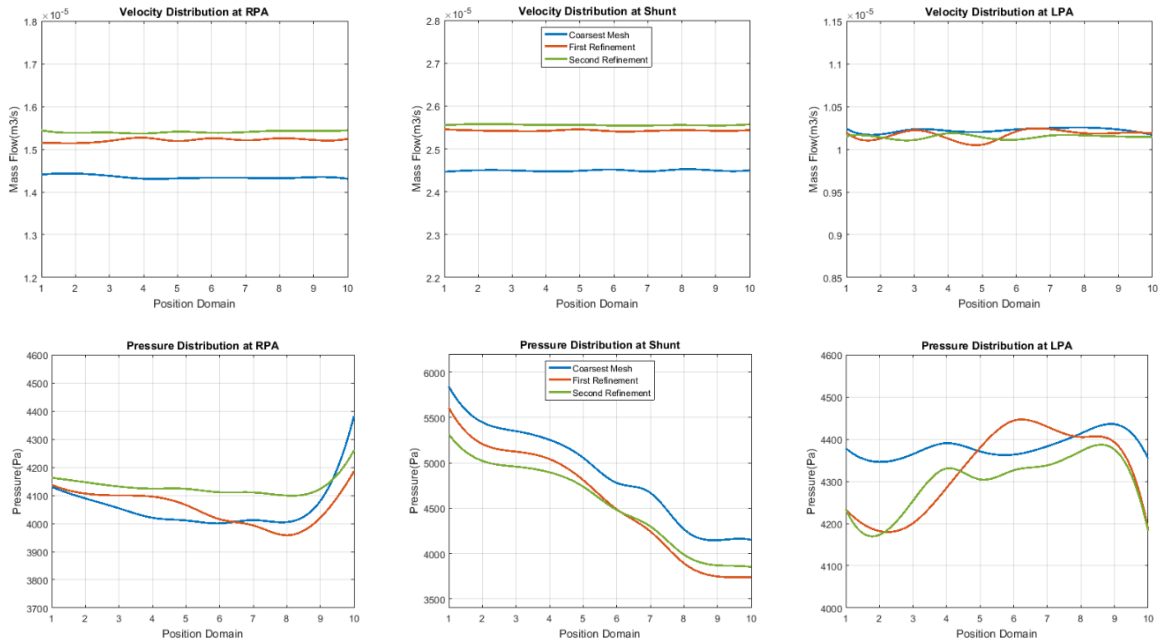


Figure 4.1 The coarsest mesh consists of 4,406,253 nodes and 2,247,165 elements; the first refined mesh consists of 8,321,809 nodes and 3,607,562 elements; and the second refined mesh consists of 8,986,225 nodes and 4,913,234 elements. The locations in the domain indicate that all computational data were taken at the center lines of the Shunt, RPA, and LPA.

# 4.2 Results of Simulation

## 4.2.1 Analysis of Simple Extruded Model of BT Shunt in Fig. 3.7

Figure 4.2 and Figure 4.3 respectively show the streamlines and Wall Shear Stress (WSS) distributions in the Simple Extruded Model of BT Shunt in Fig. 3.7. This simulation shows how the flow would distribute in various parts of the shunt and where the maximum WSS will appear. One can observe a flow pattern which has high flow rate at the bottom and relatively low flow rate on top as shown by the RPA cross-sectional velocity contours in Fig. 4.4. This flow pattern is generally observed in tubes with a T-junction. The velocity contours in the cross-section of LPA also show the same pattern as shown in Fig. 4.4. The velocity

contours are evenly distributed in LPA compared to RPA since the diameter of the pulmonary artery varies on two sides of the shunt.

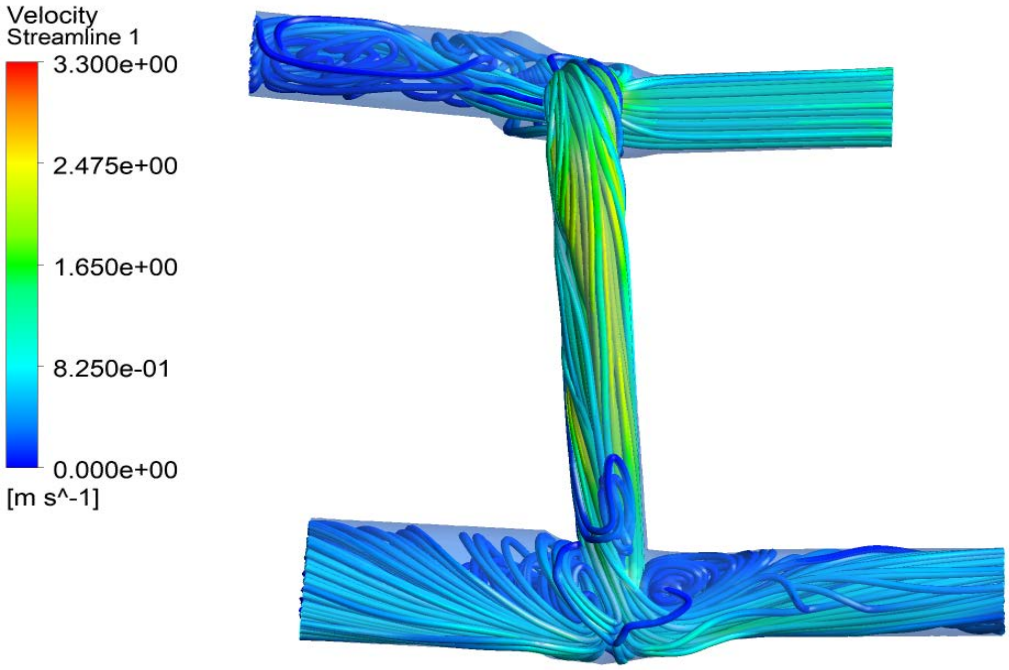


Figure 4.10 Velocity Streamlines inside the Simple Extruded Model of BT Shunt in Fig. 3.7

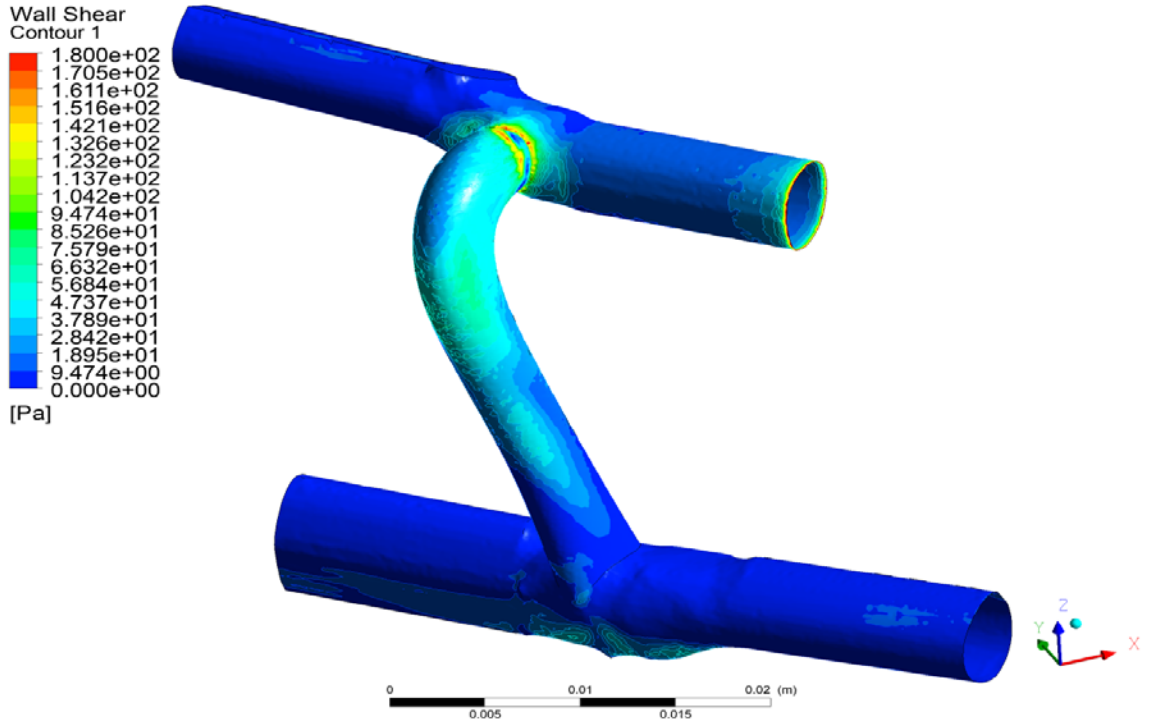


Figure 4.11 Wall Shear Stress Contours in Simple Extruded Model of BT Shunt in Fig. 3.7

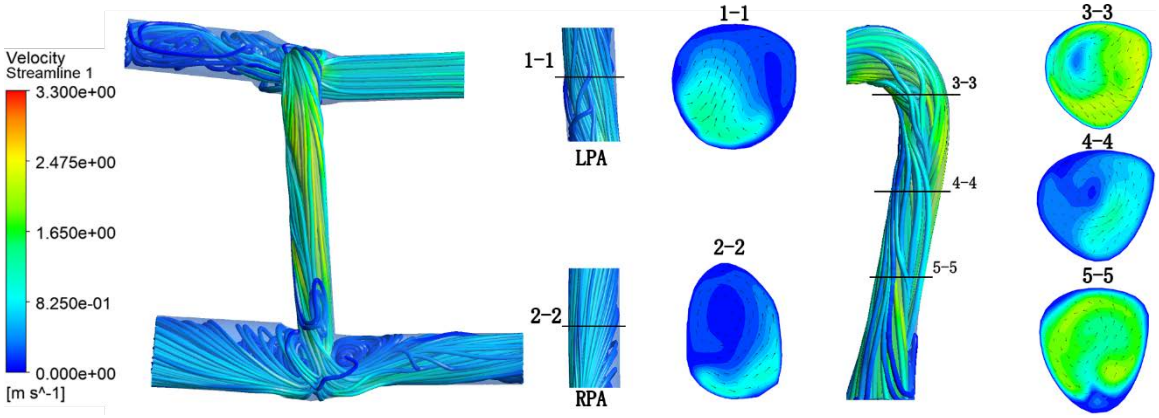


Figure4.12 Streamlines and Velocity Contours at Various Cross-Section of the Simple Extruded Model of BT Shunt in Fig. 3.7

The newly designed shunt is slightly bent near its intersection with IA in order to reduce the WSS; the average WSS reaches 14 Pa and the maximum WSS reaches 372 Pa. This improvement successfully eliminates the flow separation problem when blood flow enters

the mBT-Shunt (HHA Shunt) compared to the standard shunt which has problem in controlling the flow direction. The transition of WSS inside the shunt is also smooth which prevents the formation of thrombosis to some extent. In addition, this Simple Model shows a balanced flow distribution between RPA and LPA. The percentage difference of flow rate between LPA and RPA is 14.6% which is within the acceptable range. In the next section, the flow inside the 3D patient specific model shown in Fig. 3.8 is simulated to examine how the new shunt performs in a more realistic situation.

### 4.2.2 Flow Simulations inside Patient Specific 3-D Aorta Model with Modified BT Shunt

Table 1 gives the boundary conditions at various inflow and outflow boundaries of 3D model shown in Figure 3.8.

Table 1: Boundary Conditions for the 3-D Model

| Boundary Condition | AAO (m/s) | MPA (m/s) | IA (mmHg) | LCA (mmHg) | LSA (mmHg) | RPA (mmHg) | LPA (mmHg) | DAO (mmHg) |
|---|---|---|---|---|---|---|---|---|
| Value | 1.2 | 0.6 | 77.51 | 77.46 | 77.68 | 31.32 | 31.32 | 77.7 |

Figure 4.5-4.10 show the velocity and WSS contours inside the 3-D Model of Fig. 3.8 with boundary conditions given in Table 1. There is higher WSS near the intersection of IA and BT-Shunt as expected. Figure 4.5 shows the velocity contours at various cross-sections of the Shunt, RPA and LPA. The same flow pattern can be observed in the RPA and LPA as was observed in case of Simple Model. In the analysis, we capture a complex swirling flow in both Simple Model and 3D Model. This vortex flow is a result of the complex topology of the T-junction and the non-uniform flow in the shunt. The size of the pulmonary artery can also have an effect on the swirling flow. The LPA, which has a relatively smaller diameter, shows a stable flow pattern.

Figures 4.8-4.10 show the WSS distribution inside the geometry with various views. The 3D Model demonstrates a similar WSS as in the case of the Simple Model. It can be observed

that the variation in WSS in all regions of the model is relatively smooth and the maximum value of WSS is also smaller than that in the standard shunt. The distribution regions of high WSS decrease, which lower the probability of thrombosis. Thus, the mBTS (HHA shunt) has achieved both the objectives required of a good shunt in the simulations

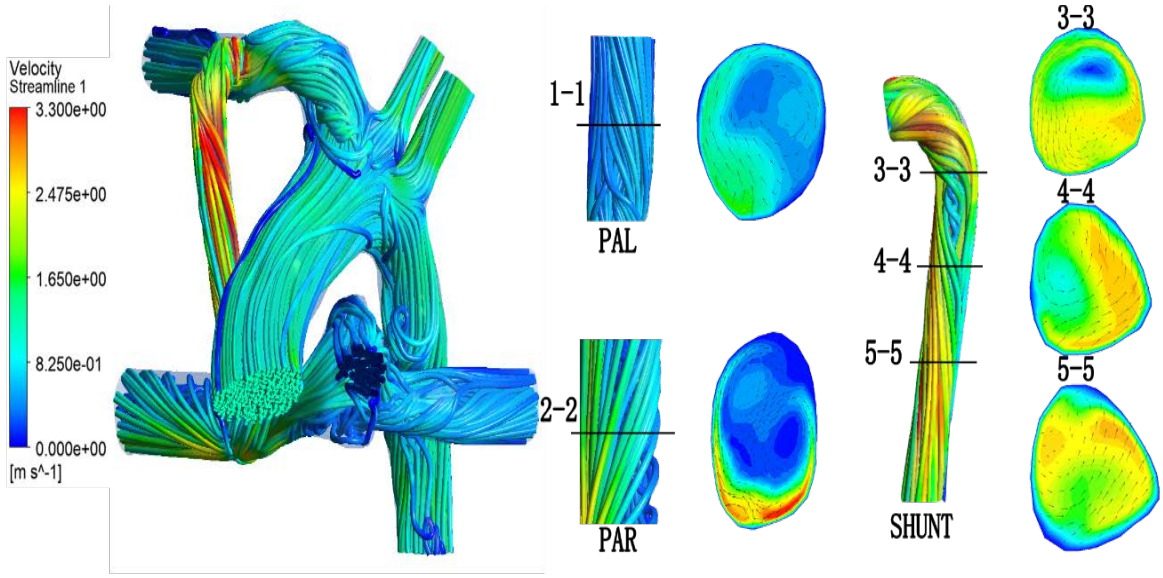


Figure 4.13 Streamlines and Velocity Contours at Various Cross-Sections of the 3-D Model

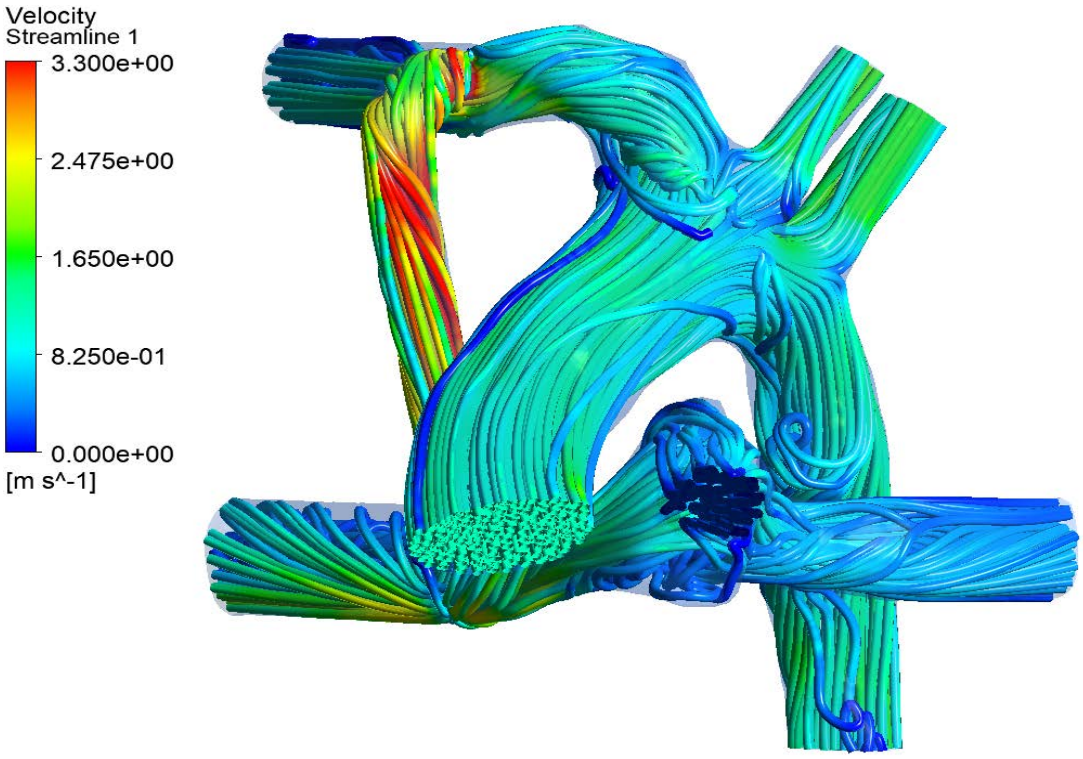


Figure 4.14 Streamlines inside the 3-D Model-Front View

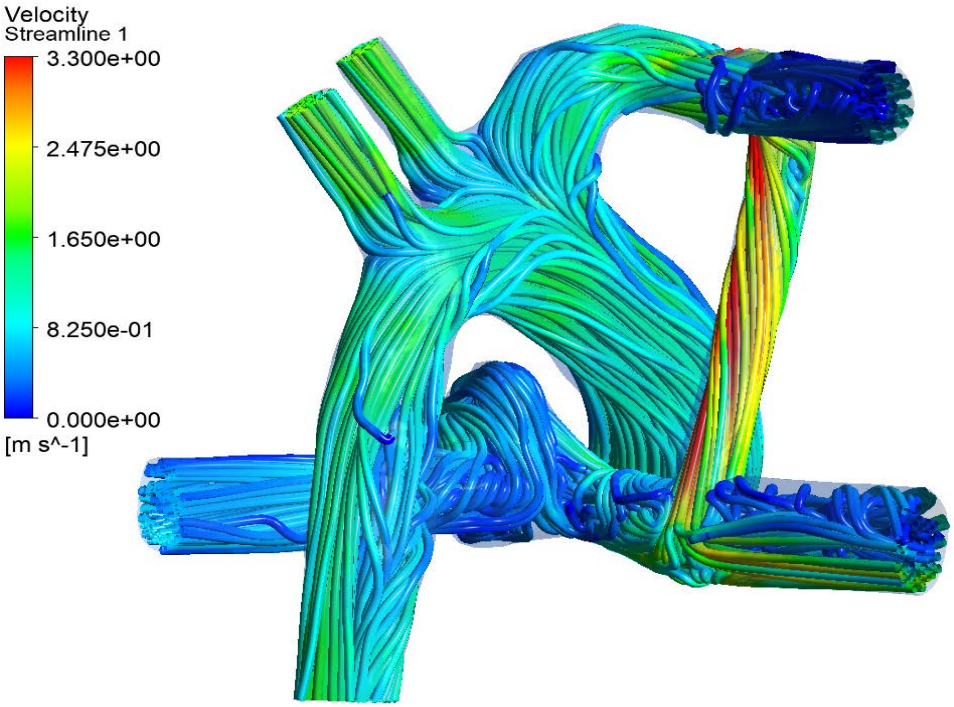


Figure 4.15 Streamlines Inside the 3-D Model-Side View

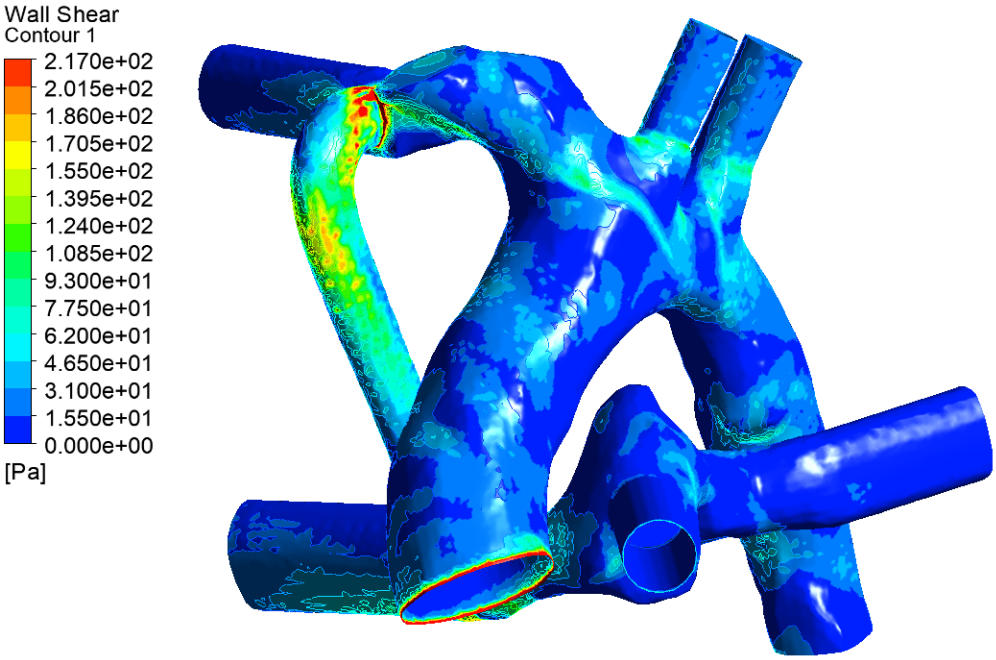


Figure 4.16 WSS Contours in the 3-D Model-Side View

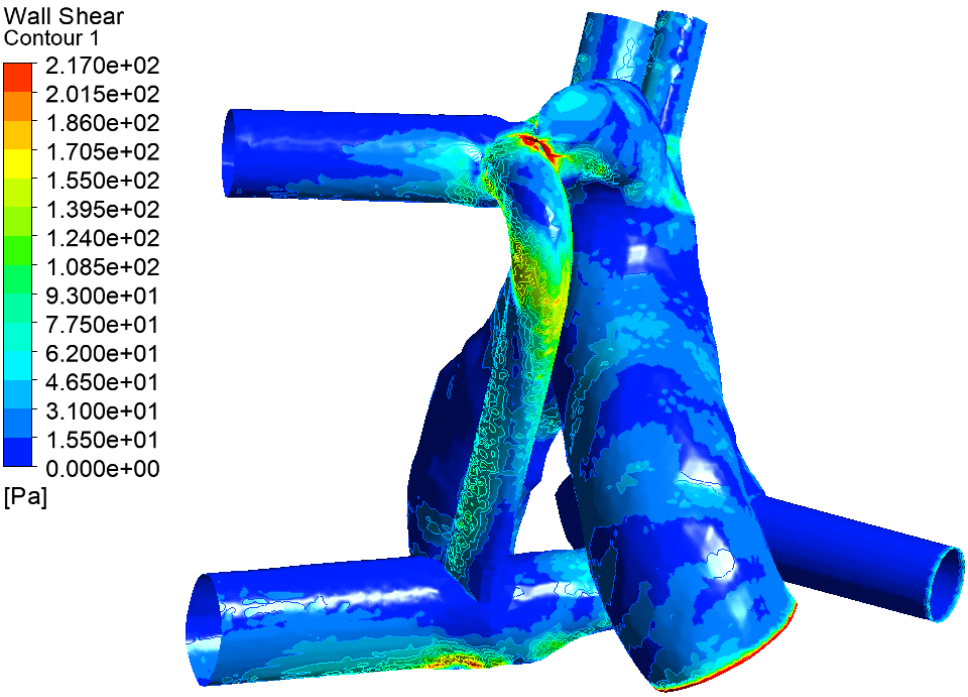


Figure 4.17 WSS Contours in the 3-D Model-Front View

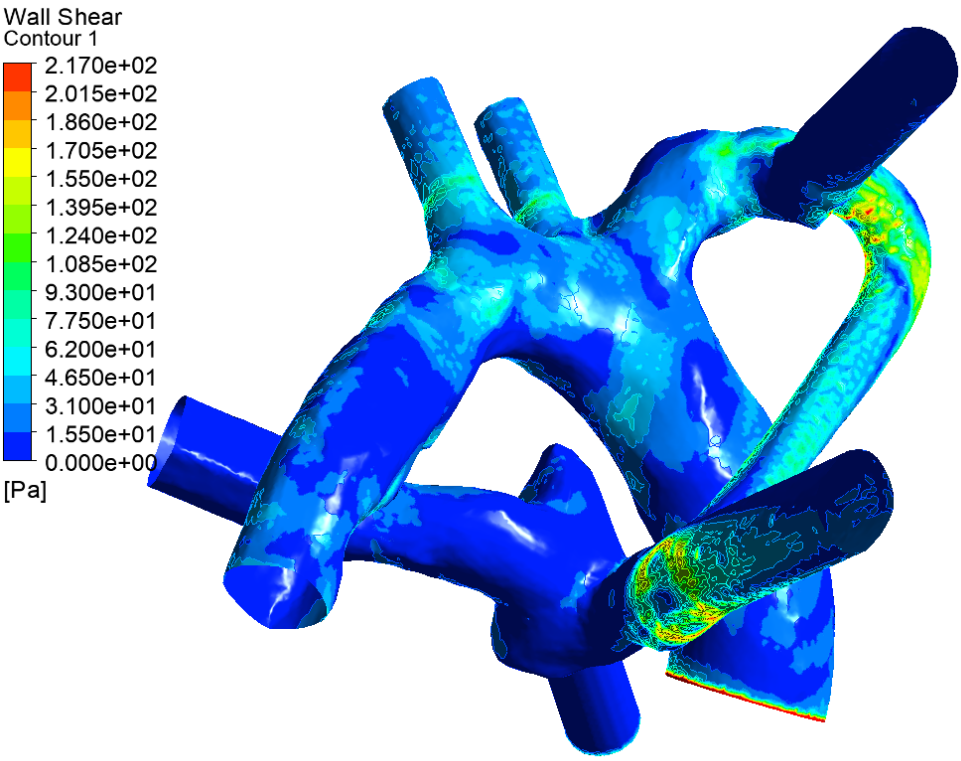


Figure 4.18 WSS Contours in the 3-D Model-Bottom View

## 4.3 Discussion

The most common problem in an installed BT-Shunt is the imbalance in the flow in RPA and LPA. The large difference in flow rates in LPA and RPA can lead to a possible failure of cardiac system due to insufficient blood flow in RPA. In our simulations, the shunt ratio is about 24% and the percentage difference in the flow rate between RPA and LPA is 8.96% which is acceptable in clinical practice. The blood flow is sufficient to left and right lungs to provide the patient enough oxygen.

However, simulation results have identified the non-uniform flow in pulmonary artery which is not desirable. The simulation showed a swirling flow in RPA which is also not desirable but is unavoidable at T-junction created by the installed shunt.

With the growth of the infants, the diameter of the Pulmonary Artery also changes and the inflow boundary condition will also change. The postoperative development of the pulmonary artery is of major concern. It is important to consider the development of PA after operation and installation of the shunt. It should be noted that the development of the pulmonary artery is largely influenced by the operation whereas the present simulation mainly focused on the pre-operational structure of the arteries.

Therefore, as a follow-up clinical data should be compared with the current simulation. This is critical for the validation of the simulation model and for determining the effectiveness of the shunt. In the present simulation, the elasticity of the vessels was neglected; the fluid structure interaction should be considered in the future work. Transient simulation with actual waveform of the heart should also be considered.

# Chapter 5 Conclusions

For steady flow simulations considered in this thesis, the mBT shunt (HHA shunt) has shown its ability in reducing the WSS with smooth variation throughout the shunt and in reducing the percentage difference in flow rate between RPA and LPA both in the Simple HHA Shunt Model and the patient specific aorta 3D Model. The main focus of this thesis was to improve the design of previously developed modified Blalock-Taussig shunt (mBTS), also designated as Hoganson-Hess-Agarwal (HHA) shunt and to evaluate its performance by attaching it to a trimmed model of an aorta of an actual patient. Simulation process involved multiple CAD software – SolidWorks and Blender for generating and assembling the solid parts. Mesh was generated inside the model by ANSYS meshing software. Reynolds-Averaged Navier-Stokes equations were solved with k-kl-ω turbulence model using the second-order accurate finite-volume method in ANSYS Fluent. A mesh independence study for the solution was conducted to ensure the accuracy of the computed solution. It was shown that the mBTS (HHA shunt) integrated with IA and PA has a smooth variation in WSS in the entire shunt with a relative low average WSS value compared to the original shunt [1] and also had low difference in flow rates (8.96%) on two sides of PA at the attachment junction of the shunt with PA. In the future, a more sophisticated and realistic simulation should be conducted to test the performance of the mBTS (HHA shunt) by comparing the simulations with available clinical data.

# Chapter 6 Future Work

In the shunt model used in Chapter 3, the ends of both IA and PA were extended so that there was no physically unrealistic reverse flow in the flow field. We also introduced MPA as a velocity inlet in Figure 3.8. However, the geometry of the MPA is not given from the CT scan, therefore we had to create its geometry separately and install it on the final 3-D Model. A more sophisticated model can be introduced with a more realistic model of MPA in order to simulate the flow in a more realistic geometry. In addition, a transient pulsatile flow simulation should be conducted to simulate the actual wave form of the heart with two peaks. All the simulations reported in the thesis consider the model to be rigid, in the future work elasticity of the model walls should be considered and simulations should be performed taking into account the fluid-structure interaction.

# References


[1] Wren C, Irving C A, Griffiths J A, et al., "Mortality in Infants with Cardiovascular Malformations," European Journal of Pediatrics, Vol. 171, No. 2, 2012, pp. 281-287.

[2] Hess, T. Agarwal, R. K., and Hoganson, D., "Numerical Simulation and Optimization of Blalock-Taussig Shunt," AJKFLUIDS2019-4784, ASME Fluids Engineering Division Summer Meeting, San Francisco, CA, July 28 – August 1, 2019.

[3] Petrucci, Orlando et al.," Risk Factors for Mortality and Morbidity after the Neonatal Blalock-Taussig Shunt Procedure", Annals of Thoracic Surgery, Vol. 92, No. 2, 2010, pp. 642 – 652.

[4] Panday S R, Karbhase J N, Rachmale G G, Hemantkumar C J, Hishikar A A. "Modified Blalock Taussig Shunt with the use of Goretex Graft," J. Postgrad Med., Vol. 28, 1982, pp.167-70.

[5] Gijsen, F. J. H, van de Vosse, F. N., and Janssen, J. D., "The Influence of the Non-Newtonian Properties of Blood on the Flow in Large Arteries: Steady Flow in a Carotid Bifurcation Model," Journal of Biomechanics, Vol. 32, No. 6, 1999, pp. 601-608.

[6] Cho, Y. I. and Kensey. K. R., "Effects of the Non-Newtonian Viscosity of Blood on Flows in a Diseased Arterial Vessel. Part 1: Steady flows," Biorheology, Vol. 28. No. 3-4, 1991, pp. 241-262.

[7] Perktold, K., R.O. Peter, et al., "Pulsatile Non-Newtonian Blood Flow in Three-Dimensional Carotid Bifurcation Models: A Numerical Study of Flow Phenomena under Different Bifurcation Angles," Journal of Biomed. Eng., Vol, 13, No. 6, 1991, pp. 507-515.

[8] ANSYS Inc., ANSYS 12.0 User Manual, 2012.

[9] Batchelor, G. K., Introduction to Fluid Mechanics, Cambridge University Press, U.K, 2000.

[10] Walters, D. K. and Cokljat, D., "A Three-Equation Eddy-viscosity Model for Reynolds-Averaged Navier-stokes for Simulations of Transitional Flows," ASME Journal of Fluids Engineering, Volume 130, December 2008.

[11]Bao, G., "Optimization of Blalock-Taussig Shunt and Anastomotic Geometry for Vascular Access Fistula Using a Genetic Algorithm," M.S. Thesis, Washington University in St. Louis, May 2015, https://openscholarship.wustl.edu/eng_etds/108

# Vita

**Zhenghao Lin**

**Degrees**: M.S., Mechanical Engineering, Washington University in St. Louis, St. Louis, MO
May 2020

B.S., Mechanical Engineering, Nanchang University, Nanchang, China
June 2018

**Publications:**

1. Lin, Z. and Agarwal, R. K., Govindarajan, V., Noah, S., Hoganson, D., and Hammer, P., "CFD Evaluation of Blood Flow in an Improved Blalock-Taussig Shunt Using Patient Specific Geometries," ASME FEDSM 2020-11129, Proceedings of the ASME 2020 Fluids Engineering Division Summer Meeting, July 12-16, 2020, Orlando, Florida, USA